IEEE Access
Multidisciplinary ⋮ Rapid Review ⋮ Open Access Journal

Received June 21, 2021, accepted July 8, 2021, date of publication July 20, 2021, date of current version July 30, 2021.

Digital Object Identifier 10.1109/ACCESS.2021.3098782

Active Capacitors With Ripple Cancellation Control for AC-DC Converter Applications

CHING-CHIEH YANG[1], (Student Member, IEEE), YANG-LIN CHEN[2], BO-YUAN CHEN[2], AND YAOW-MING CHEN[1], (Fellow, IEEE)

[1]Department of Electrical Engineering, National Taiwan University, Taipei 10617, Taiwan
[2]Delta Electronics Inc., Taoyuan 11491, Taiwan

Corresponding author: Yaow-Ming Chen (ntuymchen@ntu.edu.tw)

This work was supported in part by the Ministry of Science and Technology, Taiwan, under Grant MOST-108-2221-E-002-091-MY3.

ABSTRACT Active capacitors with long lifetime film capacitors can be adopted to replace short lifetime electrolytic capacitors to improve the reliability of the power converter. However, the conventional active capacitor suffers from the complicated control method or the need for an expensive current sensor. Based on the derived mathematical equations, a novel Ripple Cancellation Control (RCC) method for the active capacitor is proposed. The proposed RCC method is simple and can be easily realized by using analog circuits. Also, it can be applied to active capacitors implemented by different circuit topologies. Besides, a new approach for developing the mathematical model of the active capacitors implemented by different circuit topologies are also proposed. The energy storage capability and the impedance analysis by using the developed mathematical model are presented to verify the performance of the active capacitors with the proposed RCC method. Computer simulations and the hardware results are presented to validate the accuracy of the mathematical model as well as the performance of the proposed RCC method.

INDEX TERMS Active capacitors, lifetime, ripple cancellation control, energy storage capability.

I. INTRODUCTION

As the rapid growth of consumer electronics products, AC-DC power converters with the power factor correction (PFC) feature are demanded [1], [2]. However, the inherent double-line frequency voltage ripple will appear on the DC output terminal because of imbalanced input and output instantaneous power [3]–[5]. To achieve a constant DC output voltage, electrolytic capacitors, which have large capacitance, are needed to mitigating the double-line frequency voltage ripple. However, electrolytic capacitors have been criticized for their short lifetime, which also lower the reliability of AC-DC converters. Many approaches have been proposed to reduce the required capacitance so film capacitors, which have a longer lifetime, can be used for AC-DC power convertors [5]–[33].

Various power decoupling techniques have been proposed to decouple the double-line frequency input power from the DC output terminal to reduce the required output capacitance [3]–[33]. There are two types of Power decoupling circuits: passive and active. Passive power decoupling circuits are simple and easy, but low power density and poor performance are their main drawbacks [5], [6]. On the other hand, active power decoupling circuits (APDCs) required additional circuits with complex control but can achieve higher performance. Generally speaking, the operation principle of the APDC is to divert the unbalanced input-output power into an auxiliary energy storage component so the double-line frequency ripple voltage at the DC terminal can be mitigated.

In general, the circuit topology of an APDC can be divided into two parts: the original converter cell and the decoupling cell [7]–[9]. To minimize the size of power components and reduce power loss, some of the decoupling cells will share components with the original converter cell. Usually, the function of the original AC-DC converter, such as the power factor correction, will be affected by the decoupling cell [9]–[18]. On the other hand, the control of the APDC commonly increases the complexity of the original AC-DC converter. Therefore, an active capacitor has been proposed to replace the use of the APDC as well as the electrolytic capacitor [19]–[33]. Theoretically, the active capacitor can be applied to all kinds of AC-DC converters to reduce the output

The associate editor coordinating the review of this manuscript and approving it for publication was Wenjie Feng.

voltage ripple. Also, the operation of the active capacitor is independent to the original AC-DC converter.

The active capacitor is formed by a bidirectional converter and an auxiliary capacitor, which is commonly a long-lifetime film capacitor. The bidirectional converter can transfer power between the DC terminal and the auxiliary capacitor so the ripple voltage on the DC terminal can be mitigated [19]–[33].

Three types of DC-DC converters, buck, buck-boost, and boost are commonly adopted to realize the bidirectional converter inside the active capacitor [19]–[33]. The buck-type active capacitor is easy to control, but its energy storage capability is limited because of the low voltage on the auxiliary capacitor [20]–[26]. To increase the energy storage capacity, the buck-boost type active capacitor has been proposed and operated in the step-up mode with high auxiliary capacitor voltage [27]. Eventually, the boost type bidirectional converter is commonly used to realize the active capacitor [28]–[33].

Both open-loop and closed-loop control methods can be applied to the active capacitors [19]–[33]. Open-loop control methods can easily realize the steady operation of the active capacitor, but its voltage and current stress cannot be controlled [20]. The reliability issue is the main concern for an active capacitor with open-loop control. To solve this issue, many closed-loop control methods have been proposed [21]–[33]. However, a complex control loop and extra components, including a current sensor, are always required [19]–[33].

Therefore, a novel and simple control method, Ripple Cancellation Control (RCC), which can be applied to all kinds of active capacitors, is proposed in this paper. The proposed control method only requires a voltage sensor and can be easily implemented using the analog circuit. Also, a novel approach to verify the performance of the active capacitor has been proposed. Computer simulations and hardware experimental results are presented to verify the performance of the active capacitors with the proposed RCC method.

II. POWER FLOW IN AC-DC CONVERTER

Usually, the ac input voltage and current can be expressed as sinusoidal functions:

$$v_{in}(t) = V_{in}\cos(\omega t) \tag{1}$$

$$i_{in}(t) = I_{in}\cos(\omega t + \theta) \tag{2}$$

where V_{in} and I_{in} are the peak values of voltage and current, respectively, ω is the angular line frequency, and θ is the phase angle of the ac line current. By assuming that the AC-DC converter can achieve a very high power factor (PF), the line current and voltage are in phase ($\theta = 0$). Eventually, the input power of the AC-DC converter can be written as:

$$\begin{aligned} p_{in}(t) &= v_{in}(t)i_{in}(t) = \frac{1}{2}V_{in}I_{in} + \frac{1}{2}V_{in}I_{in}\cos 2\omega t \\ &= P_o + P_o\cos(2\omega t) = P_o + p_{Cbus}(t) \\ &= P_o + v_o(t)i_{Cbus}(t) = P_o + v_o(t)C_{bus}\frac{dv_o(t)}{dt} \end{aligned} \tag{3}$$

where $p_{in}(t)$ is the input power, P_o is output dc power, and $p_{Cbus}(t)$ is the instantaneous power of C_{bus}. According to (3), the input power can be divided into two parts, which are constant power P_o and the double line frequency power $p_{Cbus}(t)$. Also, the output voltage $v_o(t)$ of the AC-DC converter can be divided into two parts, which are the constant output voltage V_o and the ripple voltage $v_{o,ac}(t)$ [24]:

$$\begin{aligned} v_o(t) &= V_o + \frac{P_o}{2\omega C_{bus}V_o}\sin(2\omega t) \\ &= V_o + v_{o,ac}(t) = V_o + \frac{1}{2}\Delta V_o\sin(2\omega t) \end{aligned} \tag{4}$$

where ΔV_o is the peak to peak of the output voltage $v_o(t)$. From (4), the demanded output capacitance C_{bus} of AC-DC converter can be derived as:

$$C_{bus} = \frac{P_o}{\omega V_o \Delta V_o}. \tag{5}$$

According to (5), the required output capacitance C_{bus} is inversely proportional to the output voltage ripple for an AC-DC converter with the specified output power P_o, output voltage V_o, and angular line frequency ω. For a high output power, low output voltage, or small output voltage ripple, the electrolytic capacitor is required to accomplish the demanded performance. However, the short lifetime of electrolytic capacitor will affect the reliability of the AC-DC converter significantly. Therefore, the active capacitor has been proposed to replace the electrolytic capacitor to improve the life time of the converter.

The conceptual power flow diagram for an AC-DC converter with an active capacitor is showed in Fig. 1. The large DC-bus capacitor C_{bus} at the output terminal is always needed to mitigate the double line frequency voltage ripple caused by the input power fluctuation. By adding the active capacitor, the output capacitor C_o, which originally has the same capacitance as C_{bus}, can be dramatically reduced. The active capacitor is realized by a bidirectional converter with energy storage component, auxiliary capacitor C_a, to store and release the fluctuating power.

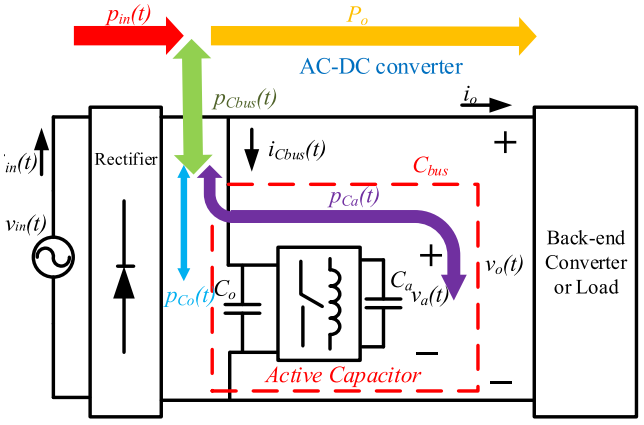

FIGURE 1. The AC-DC converter with an active capacitor.

III. ACTIVE CAPACITOR WITH RCC

In this section, the active capacitor will be introduced briefly followed by the derivation of the proposed control method.

A. ACTIVE CAPACITOR

The conceptual voltage, current, and power waveforms of the AC-DC converter with an active capacitor shown in Fig. 1 are illustrated in Fig. 2. As shown in Fig. 2, because of the in-phase input voltage $v_{in}(t)$ and current $i_{in}(t)$, the input power $p_{in(t)}$ is a double-line frequency sinusoidal function. Since the output power Po is constant, so the demanded power to the output dc bus $p_{Cbus}(t)$ should be a sinusoidal function, too. Eventually, the output voltage $v_o(t)$ has an avoidable voltage ripple with the magnitude of ΔV_o, as expressed in (4). By assuming the ideal bidirectional converter in the active capacitor with no power loss, the $p_{Cbus}(t)$ can be distributed into C_o and C_a, which can be express as:

$$p_{Cbus}(t) = p_{Ca}(t) + p_{Co}(t) \tag{6}$$

From (3) and (6), the power delivered into the auxiliary capacitor C_a, $p_{Ca}(t)$, in the active capacitor can be expressed as:

$$\begin{aligned} p_{Ca}(t) &= P_o \cos(2\omega t) - C_o v_o(t) \frac{dv_o(t)}{dt} \\ &= \left(P_o - \frac{C_o}{C_{bus}} P_o\right) \cos(2\omega t) \end{aligned} \tag{7}$$

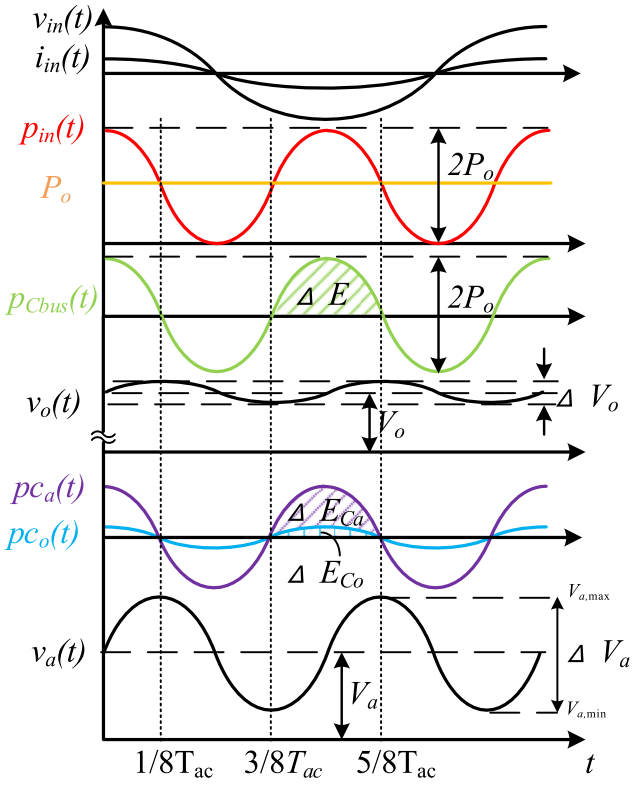

FIGURE 2. The conceptual voltage, current, and power waveforms of the AC-DC converter with an active capacitor.

where $p_{Co}(t)$ is the power of C_o. As shown in Fig. 2 and the above derived equation (7), the waveforms of the $p_{Ca}(t)$, $p_{Co}(t)$ and $p_{Cbus}(t)$ are all in phase. In addition, the voltage of the auxiliary capacitor, $v_a(t)$, can be obtained by following the similar derivation steps for (4) with the power expression shown in (6). Eventually, the following equation for $v_o(t)$ can be obtained:

$$\begin{aligned} v_a(t) &= V_a + \frac{P_o\left(1 - \frac{C_o}{C_{bus}}\right)}{2\omega C_{bus} V_a} \sin(2\omega t) \\ &= V_a + v_{a,ac}(t) = V_a + \frac{1}{2}\Delta V_a \sin(2\omega t) \end{aligned} \tag{8}$$

where V_a is the average voltage, $v_{a,ac}(t)$ is the ripple voltage, and ΔV_a is the peak to peak voltage amplitude. From (4) and (8), it can be seen that $v_o(t)$ and $v_a(t)$ are in phase as illustrated in Fig. 2. However, it should be mentioned that the derivation of (4) and (8) has ignored the harmonic components of the dc bus voltage ripple as mentioned in [4].

From (8), it is clear that $v_a(t)$ should be in phase with $v_o(t)$ to achieve the best fluctuation power absorption at the dc bus. Therefore, the most important task for the active capacitor is to control the $v_a(t)$, where the average voltage V_a and the amplitude of the sinusoidal function ΔV_a are two crucial parameters. To achieve an appropriate $v_a(t)$ control, the electric energy distribution among various capacitors should be explored.

As shown in Fig. 2, the instantaneous input power is higher than the constant output power during the time period of $3/8T_{ac}$ to $5/8T_{ac}$, where T_{ac} is the period of ac mains. The exceed power should be absorbed by the dc bus capacitor C_{bus}. From (3) and (4), the energy of C_{bus} during $3/8T_{ac}$ to $5/8T_{ac}$ time period can be expressed as:

$$\begin{aligned} \Delta E &= \int_{3T_{ac}/8}^{5T_{ac}/8} p_{Cbus}(t) = \int_{3T_{ac}/8}^{5T_{ac}/8} P_o \cos(2\omega t) \\ &= \int_{3T_{ac}/8}^{5T_{ac}/8} C_{bus}\omega V_o \Delta V_o \cos(2\omega t) = C_{bus} V_o \Delta V_o \end{aligned} \tag{9}$$

Since the active capacitor will be used to replace the original dc bus capacitor, the original energy stored C_{bus} should be delivered into the two capacitors, C_o and C_a, inside the active capacitor. Similar to (9), the absorbed energy of the active capacitor can be expressed as:

$$\begin{aligned} \Delta E &= \Delta E_{Ca} + \Delta E_{Co} = \int_{3T/8}^{5T/8} p_{Co}(t) + p_{Ca}(t) \\ &= \frac{1}{2}\left[C_o(V_{o,\max}^2 - V_{o,\min}^2) + C_a(V_{a,\max}^2 - V_{a,\min}^2)\right] \\ &= C_o V_o \Delta V_o + C_a V_a \Delta V_a \end{aligned} \tag{10}$$

From (5), (9) and (10), the output power can be expressed as:

$$P_o = \omega \Delta E_a = C_{bus}\omega V_o \Delta V_o = C_o \omega V_o \Delta V_o + C_a \omega V_a \Delta V_a \tag{11}$$

From (11), to minimize the size of capacitors, C_o and C_a, the production of V_a and ΔV_a should be maximize, since parameters P_o, V_o, ΔV_o and ω are known parameters. Also, it should be noticed that high V_a and ΔV_a values imply high voltage stress for components.

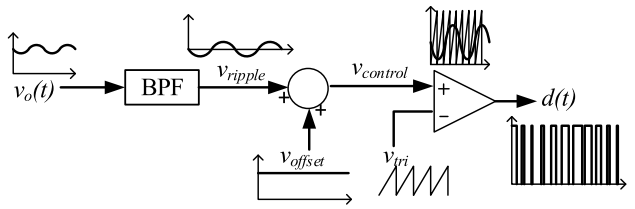

FIGURE 3. The block diagram of the proposed RCC with typical waveforms.

B. RIPPLE CANCELLATION CONTROL (RCC)

Based on the derived equations, a novel RCC method for the active capacitor is proposed. The proposed RCC method aims to cancel out the voltage ripple $v_{o,ac}(t)$ of the dc bus by controlling the auxiliary capacitor's voltage $v_a(t)$. Fig. 3 shows the conceptual control block diagram of the proposed RCC method with corresponding waveforms. The proposed RCC method is very simple and can be categorized as a feed-forward control. No conventional controllers, such as PI or PID compensators, are required.

In Fig. 3, a band-pass filter (BPF) is used to extract the ac component, v_{ripple}, of the output voltage $v_o(t)$, so its pass band should be located around the double line frequency, 120Hz. Different types of BPFs can be adopted to fulfill the task. In this paper, the BPF consists of a high pass filter and a second-order low pass filter. The high pass filter is designed to block the dc component but also to maintain sufficient gain for the double-line frequency. So the cut-off frequency is chosen to be 12 Hz. On the other hand, the second-order low pass filter is designed to suppress the 100kHz switching noise. Various types of second-order low pass filters, such as the Butterworth filter, can be adopted. In this paper, the second-order low pass filter consists of two single-pole low pass filters. The cut-off frequency of the first low pass filter is chosen to be one tenth of the switching frequency, i.e. 10kHz. In order to further attenuate the high frequency noise, another low pass filter with the cut-off frequency placed at around 1kHz is adopted.

Then an appropriate constant value, v_{offset}, which is used to control the average value of the auxiliary capacitor C_a, will be added in the loop to generate the control signal $v_{control}$ for the PWM comparator. Eventually, the gate signal $d(t)$ of the bidirectional converter inside the active capacitor will be generated to control the auxiliary capacitor's voltage, $v_a(t)$.

The main advantage of the proposed RCC method is its simplicity. Unlike other active capacitors, no current sensors implementation is needed. Also, it can be applied to different circuit topologies of active capacitors. Further design analyses will be presented in the following section.

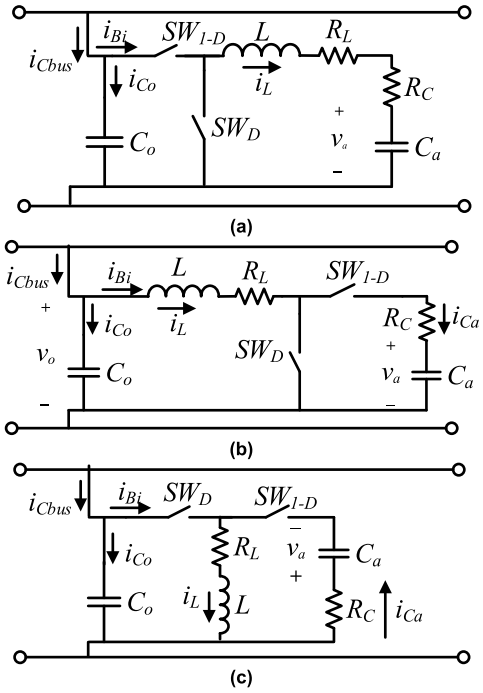

FIGURE 4. Three possible bidirectional converts for active capacitor (a) buck type; (b) boost type; (c) buck-boost type.

IV. ACTIVE CAPACITOR ANALYSIS

The objective of the active capacitor is to replace the conventional electrolytic capacitor. Therefore, the size and component counts of the bidirectional converter inside the active capacitor should be considered in the first place. In this paper, as shown in Fig. 4, only three basic types of bidirectional converters, which are buck, boost, and buck-boost, will be analyzed. Two important features of the active capacitor, power storage capability and impedance, using different types of bidirectional converters are analyzed.

A. ENERGY STORAGE CAPABILITY

To evaluate the energy storage capability of the active capacitor, an important energy storage capability index, E_X, is proposed and defined:

$$E_x = V_a \Delta V_a. \tag{12}$$

In (12), V_a can be obtained by the voltage transfer function, in term of duty ratio D, and the input terminal voltage, V_o, of the bi-directional converters. The following well-known equations are for buck, boost, and buck-boost converters, respectively.

$$V_a = DV_o \tag{13a}$$

$$V_a = \frac{1}{1-D} V_o \tag{13b}$$

$$V_a = \frac{D}{1-D} V_o \tag{13c}$$

On the other hand, ΔV_a is the difference between the possible maximum and minimum values of V_a, which is also

related to the maximum and minimum values of D and V_o as shown in the following:

$$D_{MAX} = D + \frac{1}{2}\Delta D \tag{14a}$$

$$D_{MIN} = D - \frac{1}{2}\Delta D \tag{14b}$$

$$V_{O\max} = V_o + \frac{1}{2}\Delta V_o \tag{14c}$$

$$V_{O\min} = V_o - \frac{1}{2}\Delta V_o \tag{14d}$$

where ΔD and ΔV_o are variation quantities of D and V_o, respectively. It should be mentioned that ΔV_o is the peak to peak value of the double line frequency ripple of the dc bus voltage. Also, ΔV_o is relatively small by comparing to the constant dc bus voltage. From (9), to achieve an in-phase voltage at the auxiliary capacitor, the duty ratio can be expressed as:

$$d(t) = D + \frac{1}{2}\Delta D \sin 2\omega t \tag{15}$$

As the control block diagram shown in Fig. 3, the demanded quantities of D and ΔD can be achieved by the design of the BPF voltage gain and the value of v_{offset}. By combining (12) through (15), the power index for buck, boost, and buck-boost type bidirectional converters can be derived as:

$$\begin{aligned} E_{X,buck} &= V_a \Delta V_a \\ &= DV_o \left[(D + \frac{1}{2}\Delta D)(V_o + \frac{1}{2}\Delta V_o) \right. \\ &\qquad \left. -(D - \frac{1}{2}\Delta D)(V_o - \frac{1}{2}\Delta V_o) \right] \\ &= DV_o \left(D\Delta V_o + V_o \Delta D \right) \cong V_o^2 D \Delta D \end{aligned} \tag{16}$$

$$\begin{aligned} E_{X,boost} &= V_a \Delta V_a \\ &= \frac{1}{1-D} V_o \left[\frac{1}{1-(D+\frac{1}{2}\Delta D)} (V_o + \frac{1}{2}\Delta V_o) \right. \\ &\qquad \left. - \frac{1}{1-(D-\frac{1}{2}\Delta D)} (V_o - \frac{1}{2}\Delta V_o) \right] \\ &= \frac{1}{1-D} V_o \left(\frac{\Delta D V_o}{(1-D)^2 - \frac{1}{4}\Delta D^2} \right) \\ &= \frac{\Delta D V_o^2}{(1-D)^3 - \frac{1}{4}\Delta D^2 (1-D)} \end{aligned} \tag{17}$$

$$\begin{aligned} E_{X,buck-boost} &= V_a \Delta V_a \\ &= \frac{D}{1-D} V_o \left[\frac{(D+\frac{1}{2}\Delta D)}{1-(D+\frac{1}{2}\Delta D)} (V_o + \frac{1}{2}\Delta V_o) \right. \\ &\qquad \left. - \frac{(D-\frac{1}{2}\Delta D)}{1-(D-\frac{1}{2}\Delta D)} (V_o - \frac{1}{2}\Delta V_o) \right] \\ &\cong \frac{D}{1-D} V_o \times \frac{V_o \Delta D}{(1-D)^2 - \frac{1}{4}\Delta D^2} \\ &= \frac{D \Delta D V_o^2}{(1-D)^3 - (1-D)\frac{1}{4}\Delta D^2} \end{aligned} \tag{18}$$

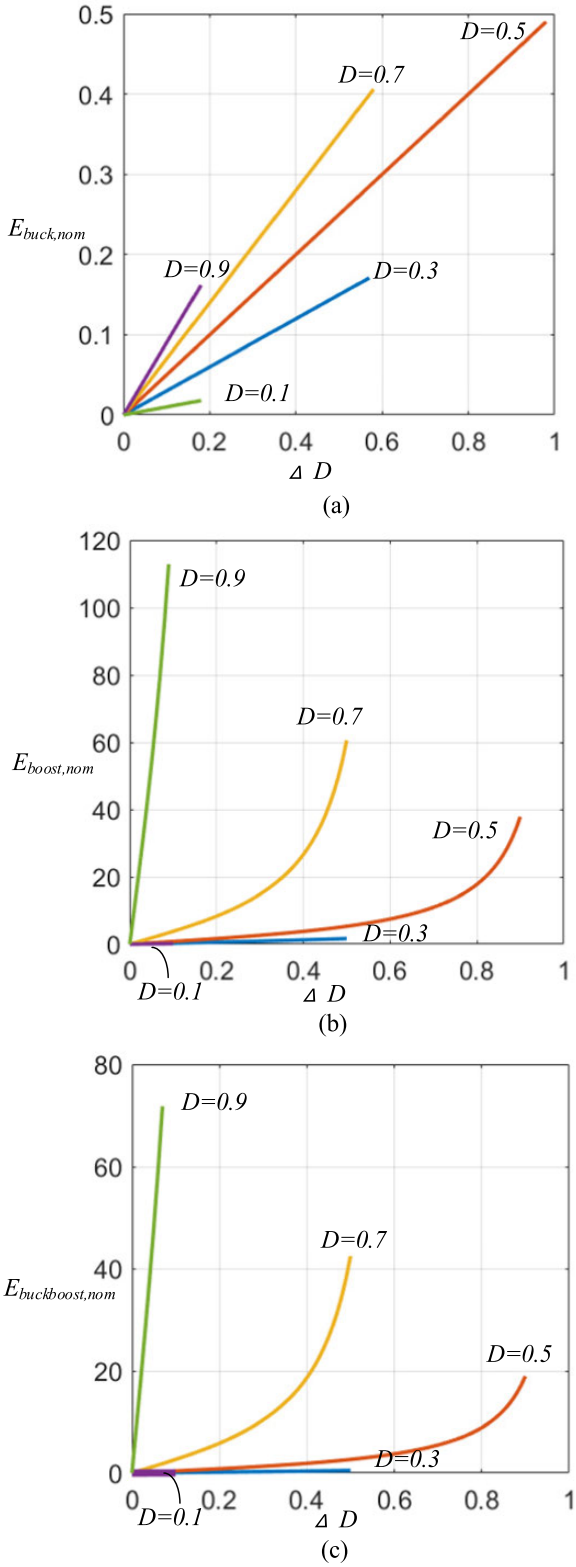

FIGURE 5. The energy storage capacity for different types of bidirectional converters (a) buck;(b) boost;(c) buck-boost.

Under the same value of V_o, the energy storage capacity index can be further normalized by dividing V_O^2,

as expressed in the following:

$$E_{x,nom} = \frac{E_x}{V_o^2} \tag{19}$$

From (15) through (19), the normalized power storage capacity index, $E_{x,nom}$, for different circuit topologies are determined by the parameters D and ΔD. Also, it should be noticed that the duty ratio should meet the following constrain:

$$0 < D \pm \left(\frac{1}{2}\Delta D\right) < 1. \tag{20}$$

Eventually, the normalized power storage capacity index for buck, boost, and buck-boost converters under different D and ΔD conditions can be illustrated as Fig. 5. It can be seen that the boost type converter can achieve higher $E_{x,nom}$ than others and is suitable for active capacitor implementation.

B. IMPEDANCE ANALYSIS

The active capacitor is expected to act like a normal capacitor, so its frequency (s-domain) analysis is essential. By using the Laplace transform, the time domain equation of a capacitor's voltage and current can be transferred into the impedance function block $Z_{co}(s)$, as shown in Fig. 6, where the input is $i_{Co}(s)$ and the output is $v_o(s)$.

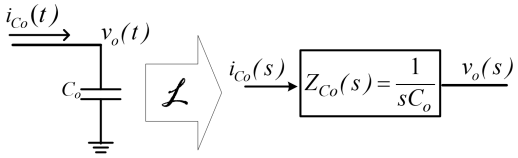

FIGURE 6. The impedance of capacitor calculated by using Laplace transform.

To analyze the performance of the active capacitor, a novel impedance model, which consists of the circuit topology with the controller, is proposed. Fig 7(a) shows the time domain function block diagram of the active capacitor with the proposed RCC method. The gate signal $d(t)$ of the bidirectional converter is produced by the PWM generator with respect to the ripple voltage $v_{contorl}(t)$ at the dc bus terminal by using the BPF. It should be mentioned that the auxiliary capacitor C_a is included inside the bidirectional converter.

Similarly, by using the Laplace transform, the s-domain function block of Fig. 7 (a) can be obtained and shown in Fig. 7(b). The impedance of the entire active capacitor, $Z_{Cbus}(s)$, is the transfer function of the input current i_{Cbus} to the dc bus voltage v_o. Because of the close-loop control of the bi-directional converter, the input current i_{Cbus} actually consists of two elements. One is the steady state current, $i_{Cbus,ss}$ produced by the open loop operation of the bidirectional converter. The other is the compensation current $i_{Cbus,com}$ generated by the negative feedback control loop. Since the $i_{Cbus,com}$ is generated according to the dc bus voltage v_o and the control loop functions of the bi-directional converter, the s-domain block diagram of the active capacitor can be drawn as shown in Fig. 7 (b). In Fig. 7 (b), $Z(s)$ is the equivalent impedance of the bi-directional converter. Because a necessary small capacitor C_o at the dc bus is included in the impedance model, the value of $Z(s)$ can be determined by the

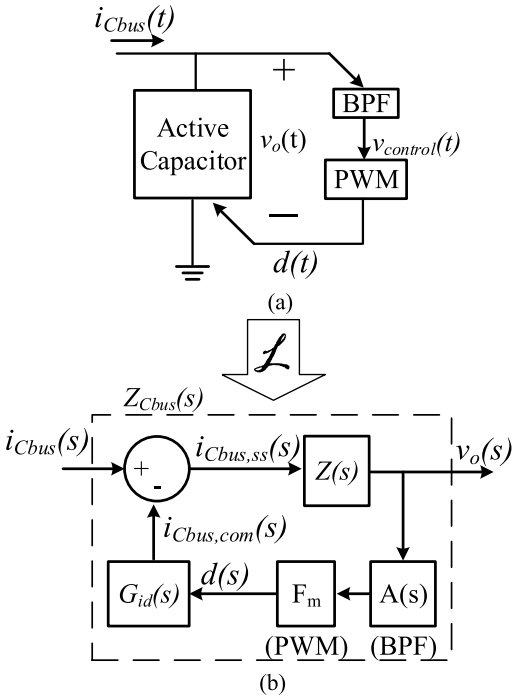

FIGURE 7. The derivation of impedance model (a) the conceptual diagram of the active capacitor with the proposed RCC; (b) the sdomain impedance model after Laplace transformation.

TABLE 1. The impedance $Z_{Bi}(s)$ and the duty-to-current $G_{id}(s)$ transfer function for different bidirectional converter.

types	$Z_{Bi}(s)$	$G_{id}(s) = \left.\frac{i_{Cbus}(s)}{d(s)}\right\|_{v_o(s)=0}$
Buck	$\frac{1}{D^2C_a}\frac{\left(\frac{s}{w_{o1}}\right)^2+\frac{s}{Q_{Bu}w_{o1}}+1}{s}$	$DV_oC_a\frac{s}{\left(\frac{s}{w_{o1}}\right)^2+\frac{s}{Q_{Bu}w_{o1}}+1}$
Boost	$\frac{(1-D)^2}{C_a}\frac{\left(\frac{s}{w_{o2}}\right)^2+\frac{s}{Q_{Bo}w_{o2}}+1}{s}$	$\frac{I_L}{(1-D)}\frac{1+\frac{s}{w_{z1}}}{\left(\frac{s}{w_{o2}}\right)^2+\frac{s}{Q_{Bo}w_{o2}}+1}$
Buck-Boost	$\frac{(1-D)^2}{D^2C_a}\frac{\left(\frac{s}{w_{o3}}\right)^2+\frac{s}{Q_{BB}w_{o3}}+1}{s}$	$\frac{DI_L}{(1-D)^2}\frac{1+\frac{s}{w_{z2}}}{\left(\frac{s}{w_{o3}}\right)^2+\frac{s}{Q_{BB}w_{o3}}+1}$

Note: Detail expressions for parameters in TABLE I are:

$$Q_{Bu} = \sqrt{\frac{L}{C_a}}\frac{1}{R_L+R_C} \quad Q_{Bo} = \sqrt{\frac{L}{C_a}}\frac{1-D}{R_L+R_C(1-D)} \quad Q_{BB} = \sqrt{\frac{L}{C_a}}\frac{1-D}{R_L+R_C(1-D)}$$

$$w_{o1} = \frac{1}{\sqrt{LC_a}} \quad w_{o2} = w_{o3} = \frac{1-D}{\sqrt{LC_a}}$$

$$w_{z1} = \frac{I_L(1-D)}{C_a\left[V_c+I_LR_c\right]} \quad w_{z2} = \frac{I_L}{C_a\left[V_a+I_L+V_o\right]}$$

bidirectional converter's impedance, $Z_{Bi}(s)$, in parallel with the small capacitor C_o, as shown in (21).

$$Z(s) = \left.\frac{v_o(s)}{i_{Cbus,ss}(s)}\right|_{d(s)=0} = \frac{1}{sC_o} // Z_{Bi}(s) \tag{21}$$

The derivation of $Z_{Bi}(s)$ for different bi-directional converters can be found in the Appendix.

TABLE 2. Specifications of the active capacitor for computer simulation.

Symbol	Quantity	Value
L	Inductor of active capacitor	300μ H
V_o	Average voltage of AC-DC converter,	208V
D	Average Duty of active capacitor	0.5
I_L	Average inductor current of active capacitor	0.02A
C_a	Auxiliary capacitor	5μ F
C_o	Output capacitor	30μ F
F_m	Peak to peak of v_{tri}	0.8
R_L	ESR of inductor	1.3 Ω
R_C	ESR of capacitor	15m Ω

Also, in Fig. 7 (b), A(s), F_m, and $G_{id}(s)$ are the s-domain functions of the BPF, PWM comparator, and the bi-directional converter's duty-to-current transfer function, respectively. It should be mentioned that A(s) and F_m remain the same, but $G_{id}(s)$ will be different for different bi-directional converters. The mathematical derivation of the $G_{id}(s)$ for different circuit topologies is presented in the Appendix. Table 1 shows the mathematical expressions of the $Z_{Bi}(s)$ and $G_{id}(s)$ for buck, boost, and buck-boost type converters, where R_L and R_C are the equivalent series resistance (ESR) of the inductor and capacitor, respectively. Eventually, the equivalent impedance of the active capacitor, $Z_{Cbus}(s)$ in s-domain can be expressed as:

$$Z_{Cbus}(s) = \frac{Z(s)}{[Z(s) \times A(s) \times G_{id}(s) \times F_m] + 1} \tag{22}$$

To validate the derivation of the impedance of the proposed active capacitor, specifications shown in Table 2 will be used for computer simulations. From (21), Table 1, and Table 2, the Bode plots, both magnitude and phase, of the impedance of those active capacitors implemented by buck, boost, and buck-boost converters can be drawn and shown in Fig. 8. It can be seen that as the frequency increases, the equivalent impedance of these active capacitors will decrease which agrees with the characteristics of a regular capacitor. Because of the zeros and poles of the bi-directional converters and their control loop, quick impedance variations exist within a specific frequency range. Also, because of the double zeros, the impedance $Z_{Bi}(s)$ has the positive slope at the high frequency range. However, because of the parallel connection with C_o, the impedance of Z(s) at high frequency range will be dominated by C_o. On the other hand, both transfer functions A(s) and $G_{id}(s)$ have negative slope at high frequency range. Eventually, at the high frequency range, the impedance magnitude of Z_{Cbus} shown in (22) can be approximated to Z(s), which is also dominated by C_o.

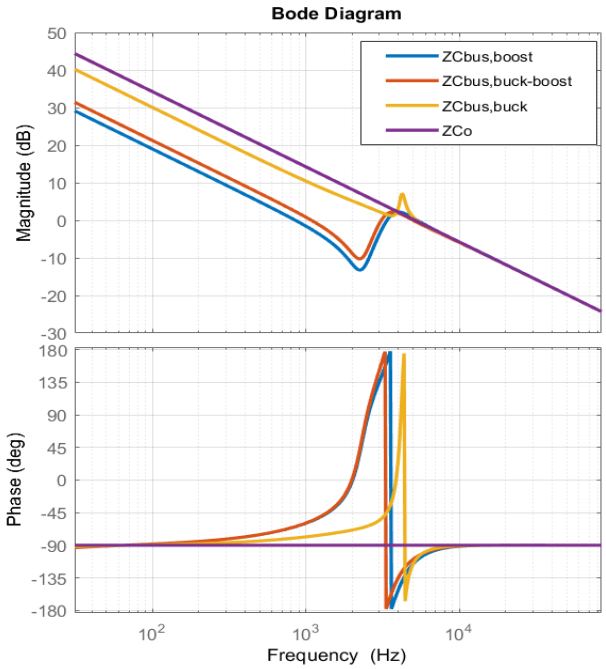

FIGURE 8. The Bode plots, both magnitude and phase, of the active capacitor impedance implemented by buck, boost, and buckboost converters.

As shown in Fig. 8, under the same line frequency, i.e. 60Hz, the boost type bi-directional converter can achieve a lower equivalent impedance which implies a higher capacitance with higher energy storage capability. It should be mentioned that different parameters in Table 1 and Table 2 will lead to different equivalent impedance plots. However, with the same parameters, the boost type bi-directional can always achieve the highest equivalent capacitance. For instance, as shown in Fig. 8 and (23), the equivalent capacitances for the buck, buck-boost, and boost type active capacitors are 50μF, 134μF, and 176μF, respectively.

$$C_{bus} = \frac{1}{2\pi f \times Z_{Cbus}(2\pi f)} \tag{23}$$

It should be mentioned that the derived impedance model shown in Fig. 7 (b) can be adopted for stability analysis of the proposed active capacitor. Conventionally, to obtain the stability judgment function from the control loop, the feedback path of the output voltage, $v_o(s)$, will be disconnected and a disturbing signal, $v_{noise}(s)$, should be injected into the compensated error amplifier. Then, the stability judgment function, $SJ(s)=v_o(s)/v_{noise}(s)$, can be obtained. The Bode plots of $SJ(s)$ function should have sufficient gain margin and phase margin to ensure the converter's stability.

Similarly, for the s-domain impedance model of the active capacitor shown in Fig. 7(b), by breaking the path from the output voltage, $v_o(s)$, but injecting a disturbing signal, $v_{noise}(s)$, into the BPF, the stability judgment function $SJ_{a-cap}(s) = v_o(s)/v_{noise}(s)$ can be obtained. It should be mentioned that the C_{bus} current, $i_{Cbus}(s)$, should be set to

zero. By applying parameters shown in Table 1, Table 2, and (21), the Bode plots of the stability judgment function $SJ_{a-cap}(s)$ for the active capacitors implemented by various bi-directional converters are shown in Fig. 9. From Fig. 9, the gain margins for boost, buck-boost, and buck type active capacitors are 18dB, 18.8dB, and 30.5dB, respectively. Also, the negative magnitude values in the whole frequency range indicate the satisfaction of phase margin. It can be seen that the presented impedance analysis in this paper is crucial for stability analysis. From Table 1, Table 2, and (21), the load value, the auxiliary capacitor C_a, and the active capacitor inductor value can be designed to meet the stability criteria.

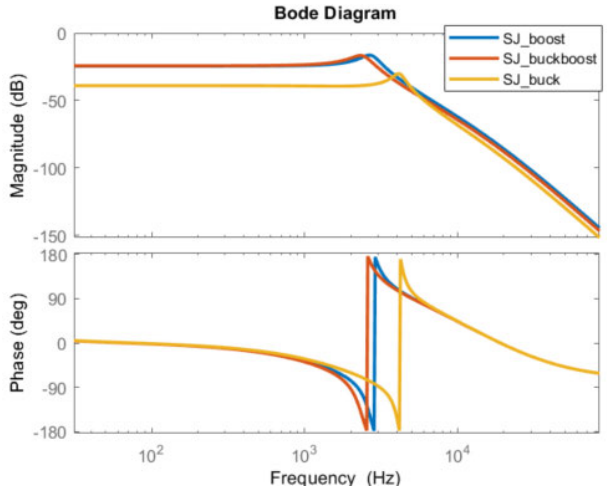

FIGURE 9. The Bode plots of the stability judgment functions of the proposed active capacitors.

V. SIMULATION RESULT

The performance of various active capacitors with the proposed RCC method can be verified by computer simulations. In this paper, the computer simulation software, Simplis, is used, and the proposed active capacitor is adopted for the AC-DC PFC converter application. Since the boost circuit topology can achieve relatively higher energy storage capacity, the boot-type active capacitor is first used to validate the correctness of the proposed mathematical model. The specifications of the PFC converter are: input voltage V_{in}=110Vrms, 60Hz; output voltage=208Vdc; output power = 110W, while those ones for the active capacitor are shown in Table 2.

Fig. 10 shows the simulation results of the boost type active capacitor with the proposed RCC for the PFC converter. In Fig. 10 (a), the voltage waveform of the auxiliary capacitor inside the active capacitor is shown on the top and the dc output voltage of the PFC converter is shown on the bottom. The average voltage of auxiliary capacitor V_a is found to be 416V which agrees with the voltage transfer function of boost using circuit parameters shown in Table 2. Also, the peak-to-peak voltage ripple of the auxiliary capacitor ΔV_a is 145V which meets the value calculated by (11).

On the other hand, by using the bode-plot function with the inherent ac sweep function build in the Simplis, the input

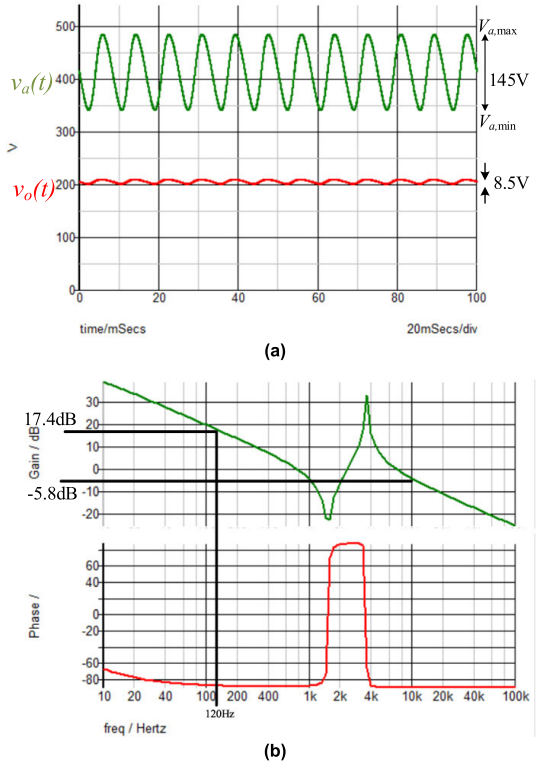

FIGURE 10. The simulation results of PFC converter with boost type active capacitor (a) voltage waveforms (b) the impedance Bode plots of the boost type active capacitor.

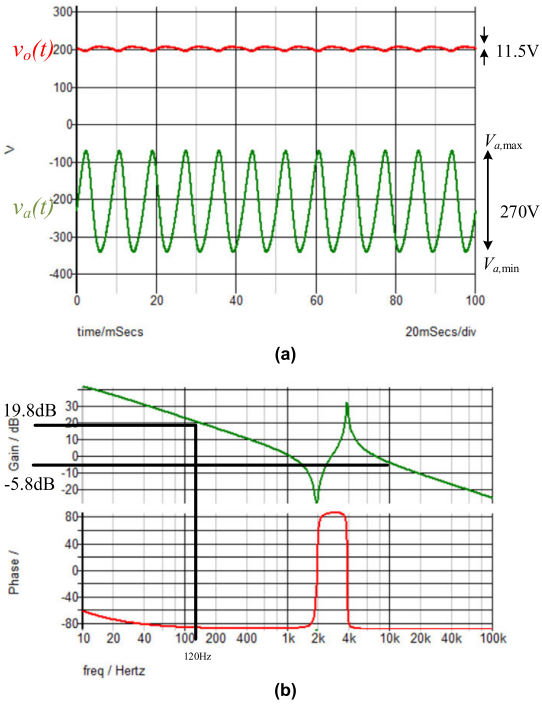

FIGURE 11. The simulation results of PFC converter with buckboost type active capacitor (a) voltage waveforms (b) the impedance Bode plots of the boost type active capacitor.

impedance of the boost type active capacitor in frequency domain can be obtained and shown in Fig. 10 (b). It can be seen that the bode plots shown in Fig. 10 (b) agree with

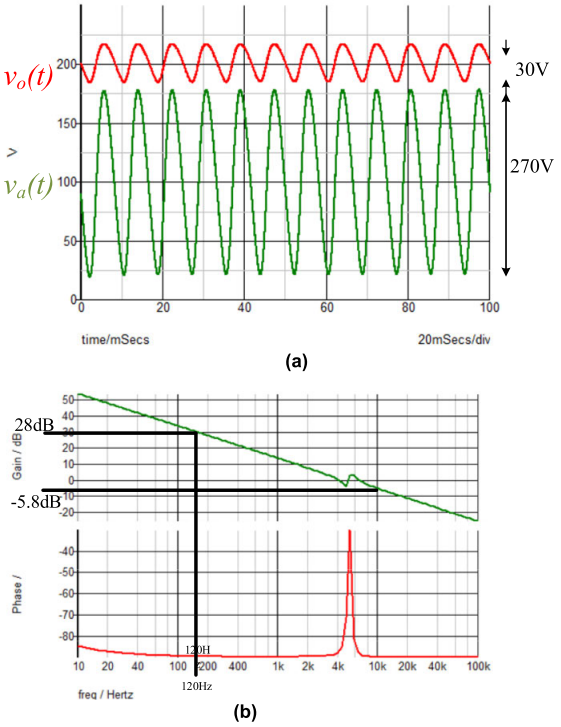

FIGURE 12. The simulation results of PFC converter with buck type active capacitor (a) voltage waveforms (b) the impedance Bode plots of the boost type active capacitor.

TABLE 3. Specifications of UCC28189.

Symbol	Quantity	Value
V_{in}	Input voltage	85~265Vac
Vo	Out voltage	208Vdc
f_{line}	Input frequency	47~63Hz
P_o	Rated power	110W
fsw	Switching frequency	120kHz
PF	Power factor	0.99
THD	Total harmonic distortion	4%
η	Full load efficiency	94.5%

the plots shown in Fig. 8, which are derived by the proposed mathematical model.

Furthermore, the equivalent impedance at 120 Hz obtained from Fig. 10 (b) is 17.4 dBΩ, which is equivalent to a 176μF capacitor operating at 120Hz. On the other hand, the measured peak to peak output voltage ripple from Fig, 10 (a) is 8.5V, which agree with value obtained from (5) using an equivalent dc bus capacitor 174μF. On the other hand, the measured impedance from Fig. 10 (b) is −5.8dBΩ, which is equivalent to a 30μF capacitor operating at 10kHz.

Similar simulation results for the buck-type and buck-boost type active capacitors are shown in Fig. 11 and Fig. 12. As shown in Fig. 11 (a), under the same operation condition, the auxiliary capacitor voltage has an average value of -208V with a 11.5 V ripple voltage, which agree with the values calculated by (11). The dc bus voltage ripple is 11.5V, which agrees with the value calculated by (5) for an equivalent 134 μF C_{bus}. On the other hand, the impedance

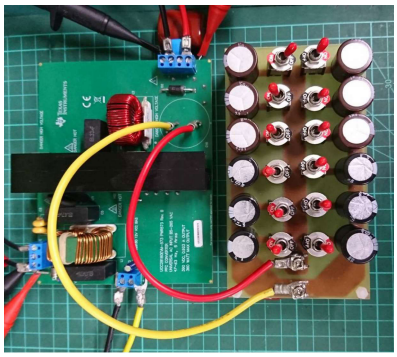

FIGURE 13. The AC-DC PFC converter with a variable capacitor bank.

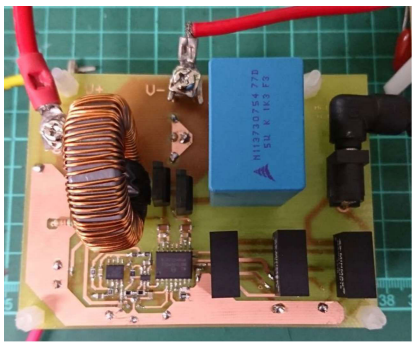

FIGURE 14. The prototype of the boost type active capacitor with the proposed RCC.

curve shown in Fig. 11 (b) agrees with the one shown in Fig. 8. Also, the 19.8dBΩ at 120Hz indicates that the buck-boost type active capacitor has an equivalent capacitance value of 134 μF which agrees with the Simplis simulation waveform obtained from Fig. 11(a). For the simulation results shown in Fig. 12, the equivalent capacitance can be found to be 55μF, which meets the voltage waveforms and impedance curve.

VI. EXPERIMENTAL RESULT

The active capacitor with the proposed RCC can be adopted for various applications. As shown in Fig. 13, an evaluation board, TI UCC28189EVM-573 AC-DC PFC converter, is adopted to verify the performance of the active capacitor with the proposed RCC. The specifications of the AC-DC PFC converter are shown in Table 3. A variable capacitor bank with manual switches is connected to the output terminal of the AC-DC converter for performance comparisons. The prototype of the boost type active capacitor is shown in Fig. 14, while its specifications are shown in Table 2.

The experimental results of the AC-DC converter using a conventional DC capacitor bus or using the prototype active capacitor are shown in Fig. 15 (a) and Fig. 15 (b), respectively. In Fig. 15(a), waveforms from top to the bottom are dc output voltage ripple $v_{o,ac}(t)$, input ac voltage $v_{in}(t)$ and current $i_{in}(t)$. The input voltage and current waveforms are in phase which implies a very good PFC feature.

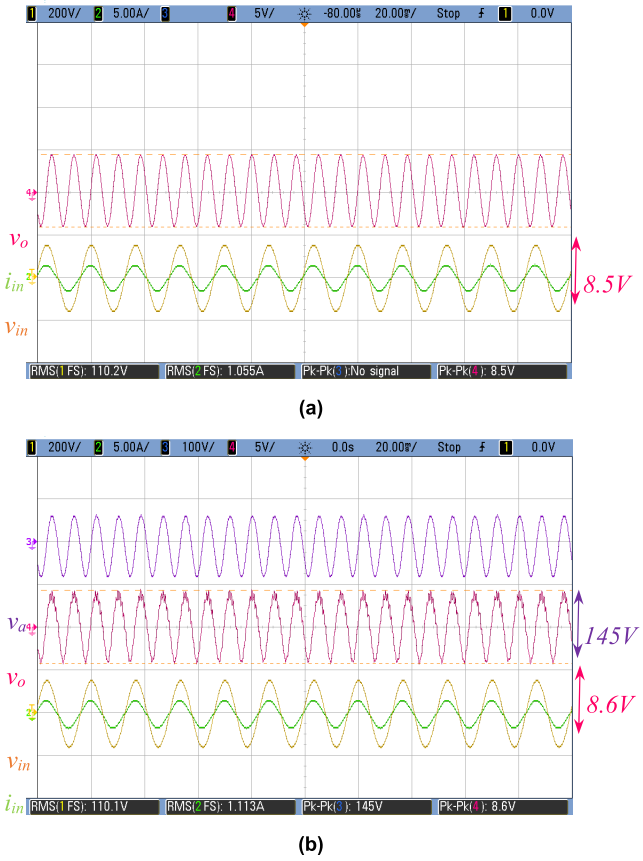

FIGURE 15. The experimental results of the AC-DC PFC converter (a) with a DC-Bus (b) with the proposed active capacitor.

To observe the voltage ripple clearly, the oscilloscope is setup at the ac mode. Under the operation condition of P_o=110W, V_o=208V, C_o=176μF, with 60Hz line frequency, the calculated output voltage ripple from (9) is ΔV_o=8.3V. As shown in Fig 15 (a), the measured dc bus voltage ripple is 8.5V, which is very close to the calculated theoretical value.

Then, the output capacitor bank is replaced by the prototype active capacitor with the propose RCC method while the AC-DC converter remains unchanged. The measured waveforms are shown in Fig. 15(b). The auxiliary capacitor voltage is shown on the top followed by the waveforms for $v_{o,ac}$, v_{in}, and i_{in}. The measured voltage ripple is 8.6V which is about the same for the one using the conventional dc bus capacitor. The voltage ripple on the auxiliary capacitor is 145V which agrees with the design procedure presented in (11) and the simulation result. In other words, the active capacitor can achieve the equivalent circuit performance of the conventional capacitor using much smaller capacitor. The auxiliary capacitor used in the active capacitor is 5μF which is about 35 times smaller than the original dc bus capacitor, 176μF.

VII. CONCLUSION

The novel RCC method for active capacitors using different circuit topologies was proposed in this paper. First, the power flow in the ac-dc converter was introduced. Then, the power flow of the active capacitor was analyzed. Based on these analyzed power flows, the novel and simple RCC method for the active capacitor was proposed. The proposed RCC is simple and can be easily realized by using analog circuits. The power density of the active capacitor can be improved since no current sensor is required. Furthermore, the proposed RCC method can achieve 35 times of the equivalent capacitance of the auxiliary capacitor C_a. Also, a new approach for developing the mathematical model of the active capacitors implemented by different circuit topologies is also proposed. The energy storage capability and the impedance analysis by using the developed mathematical model are presented to verify the performance of the active capacitors with the proposed RCC. The accuracy of the derived mathematical model and the performance of the proposed RCC method for different types of active capacitors are verified by computer simulations and hardware experiments.

APPENDIX

The mathematical equations for the boost-type bidirectional converter is presented in this section to illustrate the transfer function derivation shown in Table 2. Transfer functions for buck-boost and buck types of bidirectional converters can be obtained by using the similar derivation process presented in this section.

A. STATE-VARIABLE EQUATIONS

The boost-type bidirectional converter, as shown in Fig. 4 (b), is designed to operate in the continuous-conduction mode. The state variables, including dc bus voltage v_o, auxiliary capacitor voltage v_a, and inductor current i_L, can be expressed as a vector x:

$$x = \begin{bmatrix} v_o \\ v_a \\ i_L \end{bmatrix} \tag{A1}$$

Based on the status of the switch SW_D, either on or off, the state equations for the two circuit states can be expressed as:

$$\dot{x} = A_1 x + B_1 i_{Cbus} \quad \text{for } 0 < t < dT_s \tag{A2.a}$$
$$\dot{x} = A_2 x + B_2 i_{Cbus} \quad \text{for } dT_s < t < T \tag{A2.b}$$

where i_{Cbus} is the input of the bidirectional converter and d is the duty ratio of switch D. The state matrices A_1, B_1, A_2, and B_2 will be derived as follows.

$$A_1 = \begin{bmatrix} 0 & 0 & -\frac{1}{C_o} \\ 0 & 0 & 0 \\ \frac{1}{L} & 0 & -\frac{R_L}{L} \end{bmatrix}; \quad A_2 = \begin{bmatrix} 0 & 0 & -\frac{1}{C_o} \\ 0 & 0 & \frac{1}{C_a} \\ \frac{1}{L} & -\frac{1}{L} & -\frac{R_L + R_C}{L} \end{bmatrix};$$

$$B_1 = \begin{bmatrix} \frac{1}{C_o} \\ 0 \\ 0 \end{bmatrix}; \quad B_2 = \begin{bmatrix} \frac{1}{C_o} \\ 0 \\ 0 \end{bmatrix}$$

B. AVERAGED STATE VARIABLE EQUATIONS

The averaged state variable equation can be obtained by combining (A2.a) and (A2.b) with duty ratio as the weighting factor. It can be expressed as:

$$\dot{x} = [A_1 d + A_2(1-d)]\, x + [B_1 d + B_2(1-d)]\, i_{Cbus} \quad \text{(A3)}$$

C. AC COMPONENTS OF STATE VARIABLES

Each state variable contains a steady-state dc component X and a small-signal ac component $\tilde{x}$. Therefore, the state variables shown in (A1) can be rewritten as:

$$x = X + \tilde{x} = \begin{bmatrix} v_o \\ v_a \\ i_L \end{bmatrix} = \begin{bmatrix} V_o \\ V_a \\ I_L \end{bmatrix} + \begin{bmatrix} \tilde{v}_o \\ \tilde{v}_a \\ \tilde{i}_L \end{bmatrix} \quad \text{(A4.a)}$$

Similarly, the input current i_{Cbus} and duty ratio d can be expressed:

$$i_{Cbus} = I_{Cbus} + \tilde{i}_{Cbus} \quad \text{(A4.b)}$$

$$d = D + \tilde{d} \quad \text{(A4.c)}$$

By combining (A3) and (A4), eliminating the steady-state dc components, and neglecting those terms containing the product of $\tilde{x}$ and $\tilde{d}$, the ac components of state variable can be expressed as:

$$\begin{aligned} \dot{\tilde{x}} &= [A_1 D + A_2(1-D)]\,\tilde{x} \\ &\quad + [(A_1 - A_2)\, X + (B_1 - B_2)\, I_{Cbus}]\,\tilde{d} \\ &\quad + [B_1 + B_2(1-D)]\,\tilde{i}_{Cbus} \\ &= A\tilde{x} + B\tilde{y} \end{aligned} \quad \text{(A5)}$$

where

$$\tilde{y} = \begin{bmatrix} \tilde{i}_{Cbus} \\ \tilde{d} \end{bmatrix}; \quad A = A_1 D + A_2(1-D);$$

$$\mathrm{B} = \begin{bmatrix} B_1 + B_2(1-D) & (A_1 - A_2)\, X + (B_1 - B_2)\, I_{Cbus} \end{bmatrix}$$

D. STATE VARIABLE EQUATIONS IN S-DOMAIN

By applying the Laplace transformation, the small-signal ac components can be expressed in s-domain as:

$$sx(s) = Ax(s) + By(s) \quad \text{(A6)}$$

where

$$x(s) = \begin{bmatrix} v_o(s) \\ v_a(s) \\ i_L(s) \end{bmatrix} \text{ and } y(s) = \begin{bmatrix} i_{Cbus}(s) \\ d(s) \end{bmatrix}.$$

In (A6), different circuit topologies have different elements inside the matrices A and B. By combining (A5) through (A6), matrices A and B for the boost-type active capacitor can be expressed as:

$$A = \begin{bmatrix} 0 & 0 & -\dfrac{1}{C_o} \\ 0 & 0 & \dfrac{1-D}{C_a} \\ \dfrac{1}{L} & -\dfrac{1-D}{L} & -\dfrac{R_L + R_C(1-D)}{L} \end{bmatrix}$$

$$\mathrm{B} = \begin{bmatrix} \dfrac{1}{C_o} & 0 \\ 0 & -\dfrac{I_L}{C_a} \\ 0 & \dfrac{V_a + R_C I_L}{L} \end{bmatrix} \quad \text{(A7)}$$

E. IMPEDANCE TRANSFER FUNCTION DERIVATION

The derivation of various transfer functions of the bi-directional converter can be achieved by using the above developed small signal state variable equations. For instance, the impedance of active capacitor is defined as the transfer function of $v_o(s)$ to $i_{Cbus}(s)$ while neglecting the disturbance of $d(s)$ by setting it to be zero.

From the s-domain state variable equations (A6) and (A7), the following equations can be obtained:

$$sv_o(s) = -\frac{1}{C_o} i_L(s) + \frac{1}{C_o} i_{Cbus}(s) \quad \text{(A8.a)}$$

$$sv_a(s) = \frac{1-D}{C_a} i_L(s) \quad \text{(A8.b)}$$

$$si_L(s) = \frac{1}{L} v_o(s) - \frac{1-D}{L} v_a(s) - \frac{R_L + R_C\,(1-D)}{L} i_L(s) \quad \text{(A8.c)}$$

It should be mentioned that (A8.a) is the current equation for the connecting node of L and C_o as shown in Fig. 4(b). On the other hand, the inductor current will flow into switches SW_D and SW_{1-D} according to the portion of conduction time, i.e. duty ration D or *1-D*. Therefore, (A8.b) reveals the fact that switch $\mathrm{SW_{1-D}}$ is connected in series with the auxiliary capacitor C_a. Also, (A8.c) can be obtained directly by applying the Kirchhoff Voltage Law to the loop of C_o, L, and C_a.

From (A8.a) through (A8.c) the impedance of the active capacitor can be obtained:

$$\mathrm{Z}(s) = \left.\frac{v_o(s)}{i_{Cbus}(s)}\right|_{d(s)=0} = \frac{1}{sC_o + \dfrac{C_a}{(1-D)^2} \dfrac{s}{\left(\frac{s}{w_{o2}}\right)^2 + \frac{s}{Q_{\mathrm{Bo}} w_{o2}} + 1}} \quad \text{(A9)}$$

where

$$w_{o2} = \frac{1-D}{\sqrt{LC_a}}; \quad Q_{\mathrm{Bo}} = \sqrt{\frac{L}{C_a}} \frac{1-D}{R_L + R_C(1-D)}$$

By examining (A9), it can be found that the active capacitor impedance $\mathrm{Z}(s)$ is the summation of two parallel connected impedances, sC_o and the equivalent impedance Z_{Bi} of the bidirectional converter. Therefore, (A10) can be rewritten as:

$$\mathrm{Z}(s) = \left.\frac{v_o(s)}{i_{Cbus,ss}(s)}\right|_{d(s)=0} = \frac{1}{sC_o} // Z_{Bi}(s) \quad \text{(A10)}$$

where the impedance of the bidirectional converter is:

$$Z_{Bi}(s) = \left.\frac{v_o(s)}{i_{Bi}(s)}\right|_{d(s)=0} = \frac{(1-D)^2}{C_a} \frac{\left(\frac{s}{w_{o2}}\right)^2 + \frac{s}{Q_{\mathrm{Bo}} w_{o2}} + 1}{s} \quad \text{(A11)}$$

The impedance of buck type and buck-boost type active capacitor can be derived by using the similar approach. Eventually, the equivalent impedance for different types of bidirectional converter shown in Table 1 can be obtained.

F. TRANSFER FUNCTION DERIVATION FOR $G_{id}(s)$

The derivation procedure of $G_{id}(s)$ is similar to the one for $Z_{Bi}(s)$. The $G_{id}(s)$ is the transfer function of d(s) to $i_{Cbus}(s)$ while neglecting the disturbance of $v_o(s)$ by setting it to be zero. Similarly, the following equations can be obtained from (A6) and (A7):

$$0 = -\frac{1}{C_o} i_L(s) + \frac{1}{C_o} i_{Cbus}(s) \tag{A13.a}$$

$$sv_a(s) = \frac{1-D}{C_a} i_L(s) - \frac{I_L}{C_a} d(s) \tag{A13.b}$$

$$si_L(s) = -\frac{1-D}{L} v_a(s) - \frac{R_L + R_C(1-D)}{L} i_L(s) + \frac{V_a + R_C I_L}{L} d(s) \tag{A13.c}$$

From (A13), the $G_{id}(s)$ can be obtained and shown as:

$$G_{id}(s) = \left.\frac{i_{Cbus}(s)}{d(s)}\right|_{v_o(s)=0} = \frac{I_L}{(1-D)} \frac{1 + \frac{s}{w_{z1}}}{\left(\frac{s}{w_{o2}}\right)^2 + \frac{s}{Q_{Bo} w_{o2}} + 1} \tag{A14}$$

where

$$w_{Z1} = \frac{I_L(1-D)}{C_a[V_c + I_L R_c]};$$

The $G_{id}(s)$ of buck type and buck-boost type active capacitor can be derived by using a similar approach. Eventually, the parameters are shown in Table 1 can be obtained.

REFERENCES

[1] O. García, J. A. Cobos, R. Prieto, and J. Uceda, "Single phase power factor correction: A survey," *IEEE Trans. Power Electron.*, vol. 18, no. 3, pp. 749–755, May 2003.
[2] L. Huber, Y. Jang, and M. M. Jovanovic, "Performance evaluation of bridgeless PFC boost rectifiers," *IEEE Trans. Power Electron.*, vol. 23, no. 3, pp. 1381–1390, May 2008.
[3] L. Gu, X. Ruan, M. Xu, and K. Yao, "Means of eliminating electrolytic capacitor in AC/DC power supplies for LED lightings," *IEEE Trans. Power Electron.*, vol. 24, no. 5, pp. 1399–1408, May 2009.
[4] H. Zhang, X. Li, B. Ge, and R. S. Balog, "Capacitance, DC voltage utilizaton, and current stress: Comparison of double-line frequency ripple power decoupling for single-phase systems," *IEEE Ind. Electron. Mag.*, vol. 11, no. 3, pp. 37–49, Sep. 2017.
[5] H. Wang and F. Blaabjerg, "Reliability of capacitors for DC-link applications in power electronic converters—An overview," *IEEE Trans. Ind. Appl.*, vol. 50, no. 5, pp. 3569–3578, Sep./Oct. 2014.
[6] M. Vasiladiotis and A. Rufer, "Dynamic analysis and state feedback voltage control of single-phase active rectifiers with DC-link resonant filters," *IEEE Trans. Power Electron.*, vol. 29, no. 10, pp. 5620–5633, Oct. 2014.
[7] M. A. Vitorino, L. F. S. Alves, R. Wang, and M. B. de Rossiter Correa, "Low-frequency power decoupling in single-phase applications: A comprehensive overview," *IEEE Trans. Power Electron.*, vol. 32, no. 4, pp. 2892–2912, Apr. 2017.
[8] Y. Sun, Y. Liu, M. Su, W. Xiong, and J. Yang, "Review of active power decoupling topologies in single-phase systems," *IEEE Trans. Power Electron.*, vol. 31, no. 7, pp. 4778–4794, Jul. 2016.
[9] H. Sun, H. Wang, and W. Qi, "Automatic power decoupling controller of dependent power decoupling circuit for enhanced transient performance," *IEEE Trans. Ind. Electron.*, vol. 66, no. 3, pp. 1820–1831, Mar. 2019.
[10] H. Li, K. Zhang, H. Zhao, S. Fan, and J. Xiong, "Active power decoupling for high-power single-phase PWM rectifiers," *IEEE Trans. Power Electron.*, vol. 28, no. 3, pp. 1308–1319, Mar. 2013.
[11] H. Wang, M. Liserre, and F. Blaabjerg, "Toward reliable power electronics: Challenges, design tools, and opportunities," *IEEE Ind. Electron. Mag.*, vol. 7, no. 2, pp. 17–26, Jun. 2013.
[12] Y. Tang and F. Blaabjerg, "A component-minimized single-phase active power decoupling circuit with reduced current stress to semiconductor switches," *IEEE Trans. Power Electron.*, vol. 30, no. 6, pp. 2905–2910, Jun. 2015.
[13] Y. Kai, X. Ruan, X. Mao, and Z. Ye, "Reducing storage capacitor of a DCM boost PFC converter," *IEEE Trans. Power Electron.*, vol. 27, no. 1, pp. 151–160, Jan. 2012.
[14] Y. Tang, F. Blaabjerg, P. C. Loh, C. Jin, and P. Wang, "Decoupling of fluctuating power in single-phase systems through a symmetrical half-bridge circuit," *IEEE Trans. Power Electron.*, vol. 30, no. 4, pp. 1855–1865, Apr. 2015.
[15] Y. Y. S. Liu, M. Su, X. Li, and J. Yang, "Active power decoupling method for single-phase current-source rectifier with no additional active switches," *IEEE Trans. Power Electron.*, vol. 31, no. 8, pp. 5644–5654, Aug. 2016.
[16] V. Michal, "Switched-mode active decoupling capacitor allowing volume reduction of the high-voltage DC filters," *IEEE Trans. Power Electron.*, vol. 31, no. 9, pp. 6104–6111, Sep. 2016.
[17] Y. Zhang, Y. Huang, P. Fang, X. Gao, Y. Yang, and J. Liu, "Capacitors voltage ripple complementary control on three-level boost fed single-phase VSI with enhanced power decoupling capability," *IEEE Trans. Power Electron.*, early access, Apr. 13, 2021, doi: 10.1109/TPEL.2021.3072869.
[18] H. Li, S. Li, and W. Xiao, "Single-phase LED driver with reduced power processing and power decoupling," *IEEE Trans. Power Electron.*, vol. 36, no. 4, pp. 4540–4548, Apr. 2021.
[19] G. Kafanas, M. R. Jeffrey, and X. Yuan, "Variable structure control for active power decoupling topologies," in *Proc. 8th IET Int. Conf. Power Electron., Mach. Drives (PEMD)*, Apr. 2016, pp. 1–6.
[20] R. Wang, F. Wang, D. Boroyevich, R. Burgos, R. Lai, P. Ning, and K. Rajashekara, "A high power density single-phase PWM rectifier with active ripple energy storage," *IEEE Trans. Power Electron.*, vol. 26, no. 5, pp. 1430–1443, May 2011.
[21] S. Bayhan, "Grid voltage sensorless model predictive control for a single-phase T-Type rectifier with an active power decoupling circuit," *IEEE Access*, vol. 9, pp. 19161–19174, 2021.
[22] K.-H. Chao, P.-T. Cheng, and T. Shimizu, "New control methods for single phase PWM regenerative rectifier with power decoupling function," in *Proc. Int. Conf. Power Electron. Drive Syst. (PEDS)*, Nov. 2009, pp. 1091–1096.
[23] S. Sadrian and J. Wang, "Buck-plus-unfolder as the superior active power decoupling solution for 400 Vdc/kW-level applications," *IEEE Open J. Power Electron.*, vol. 1, pp. 260–272, Jul. 2020.
[24] H. Yuan, S. Li, S.-C. Tan, and S. Y. Hui, "Sensor count reduction for single-phase converters with an active power buffer using algebraic observers," *IEEE Trans. Ind. Electron.*, early access, Nov. 19, 2020, doi: 10.1109/TIE.2020.3037993.
[25] M. Chen, Z. Ye, Y. Chen, and D. Xu, "Zero-voltage-switching single-phase full-bridge inverter with active power decoupling," *IEEE Trans. Power Electron.*, vol. 36, no. 1, pp. 571–582, Jan. 2021.
[26] N. Deshmukh, S. Prabhakar, and S. Anand, "Power loss reduction in buck converter based active power decoupling circuit," *IEEE Trans. Power Electron.*, vol. 36, no. 4, pp. 4316–4325, Apr. 2021.
[27] M. Jang, M. Ciobotaru, and V. G. Agelidis, "A single-stage fuel cell energy system based on a buck–boost inverter with a backup energy storage unit," *IEEE Trans. Power Electron.*, vol. 27, no. 6, pp. 2825–2834, Jun. 2012.
[28] X. Zhang, X. Ruan, H. Kim, and C. K. Tse, "Adaptive active capacitor converter for improving stability of cascaded DC power supply system," *IEEE Trans. Power Electron.*, vol. 28, no. 4, pp. 1807–1816, Apr. 2013.
[29] S.-Y. Lee, Y.-L. Chen, Y.-M. Chen, and K. H. Liu, "Development of the active capacitor for PFC converters," in *Proc. IEEE Energy Convers. Congr. Expo. (ECCE)*, Sep. 2014, pp. 1522–1527.
[30] H. Watanabe, J. Itoh, and Q. Roudier, "Single-phase power decoupling technique utilizing Hybrid method with passive and active power decoupling," in *Proc. IEEE Int. Power Electron. Appl. Conf. Expo. (PEAC)*, Nov. 2018, pp. 1–6.
[31] C.-C. Yang, Y.-L. Chen, and Y.-M. Chen, "Active capacitor with ripple-based duty cycle modulation for AC-DC applications," in *Proc. IEEE Appl. Power Electron. Conf. Expo. (APEC)*, Mar. 2016, pp. 558–563.

[32] Y. Yang, X. Ruan, L. Zhang, J. He, and Z. Ye, "Feed-forward scheme for an electrolytic capacitor-less AC/DC LED driver to reduce output current ripple," *IEEE Trans. Power Electron.*, vol. 29, no. 10, pp. 5508–5517, Oct. 2014.
[33] W. Cai, B. Liu, S. Duan, and L. Jiang, "An active low-frequency ripple control method based on the virtual capacitor concept for BIPV systems," *IEEE Trans. Power Electron.*, vol. 29, no. 4, pp. 1733–1745, Apr. 2014.

CHING-CHIEH YANG (Student Member, IEEE) received the B.S. degree in electrical engineering from the National Tsing Hua University, Hsinchu, Taiwan, in 2014. He is currently pursuing the Ph.D. degree in electrical engineering with the National Taiwan University, Taipei, Taiwan. From September 2019 to August 2020, he was a Visiting Scholar at Future Energy Electronics Center (FEEC), part of The Bradley Department of Electrical and Computer Engineering, Virginia Polytechnic Institute and State University, VA, USA. His research interests include active decoupling circuit and power factor correction. He received the fellowship from the Ministry of Science and Technology, Taiwan.

YANG-LIN CHEN received the B.S. and Ph.D. degrees in electrical engineering from the National Taiwan University, Taipei, Taiwan, in 2010 and 2016, respectively. In 2016, he joined Delta Electronics Inc., where he is currently an Electrical Principal Engineer with Electric Vehicle Solution Business Group. His research interests include power electronics, magnetics design, and simulation.

BO-YUAN CHEN was born in Taichung, Taiwan, in 1996. He received the B.S. degree from the National Chung Cheng University, Chiayi, Taiwan, in 2018, and the M.S. degree from the National Taiwan University, Taipei, Taiwan, in 2020.

In 2021, he joined Delta Electronics. His research interests include GaN-based inverters, quasi-resonant flyback, and active capacitors.

YAOW-MING CHEN (Fellow, IEEE) received the B.S. degree in electrical engineering from the National Cheng Kung University, Tainan, Taiwan, in 1989, and the M.S. and Ph.D. degrees in electrical engineering from the University of Missouri, Columbia, MO, USA, in 1993 and 1997, respectively.

From 1997 to 2000, he was with I-Shou University, Taiwan, as an Assistant Professor. From 2000 to 2008, he was with the National Chung Cheng University, Taiwan. In 2008, he joined the National Taiwan University, where he is currently a Professor with the Department of Electrical Engineering. His research interests include power electronic converters and renewable energy.